IEEE Access
Multidisciplinary ⋮ Rapid Review ⋮ Open Access Journal

Received December 27, 2020, accepted January 5, 2021, date of publication January 8, 2021, date of current version January 19, 2021.

*Digital Object Identifier 10.1109/ACCESS.2021.3050196*

# Identification Method of Coal and Coal Gangue Based on Dielectric Characteristics

**YONGCUN GUO[1,2,3], XINQUAN WANG[1,2], SHUANG WANG[1,2,3], KUN HU[1,2,3], AND WENSHAN WANG[1,3]**

[1]School of Mechanical Engineering, Anhui University of Science and Technology, Huainan 232001, China
[2]State Key Laboratory of Mining Response and Disaster Prevention and Control in Deep Coal Mines, Anhui University of Science and Technology, Huainan 232001, China
[3]Mining Intelligent Technology and Equipment Provinces and Ministries jointly build a Collaborative Innovation Center, Anhui University of Science and Technology, Huainan 232001, China

Corresponding author: Xinquan Wang (wxq995@126.com)

This work was supported in part by the National Natural Science Foundation of China under Grant 51874004 and Grant 51904007, in part by the Anhui Province Science and Technology Major Special Funding Project under Grant 18030901049, in part by the Anhui Natural Science Foundation Project under Grant 1908085QE227, and in part by the Key Research and Development Program of Anhui Province under Grant 202004a07020043.

**ABSTRACT** To solve the problems of the difficult feature extraction, poor feature credibility and low recognition accuracy of coal and gangue, this paper utilizes the difference in the dielectric properties of coal and gangue and in combination with a support vector machine (SVM) to propose a recognition method based on the dielectric characteristics of coal and gangue. The influence rule of the edge effect of the electrode plate on the capacitance value is analyzed when the thickness of the electrode plate changes. By changing the frequency and voltage of the excitation source, curves of the dielectric constant of coal and gangue versus frequency and voltage are obtained. Combined with the Kalman filter, the adaptive noise complete set empirical mode decomposition (CEEMDAN) denoising method is improved, which results in a signal with a higher signal-to-noise ratio and lower root mean square error after denoising. The effective value and frequency of the denoised response signal are extracted to construct the feature vector set to form the training set and test set. The data of the training set are input into the SVM to train the intelligent classification model, the test set is used to test the SVM classification effect, and the classification accuracy is 100%. Unlike these of the probabilistic neural network (PNN) intelligent classification model and the learning vector quantization (LVQ) neural network classification model, the recognition and classification accuracies of the three can reach 100%, but the classification speed of SVM is the fastest, only taking 0.007916 s, which fully reflects the feasibility and efficiency of the capacitance method in identifying coal gangue. In this paper, the capacitance method and SVM are applied to identify coal and gangue, and accurate and efficient identification results are obtained, providing a new feasible solution for research on coal gangue identification.

**INDEX TERMS** Coal gangue, edge effect, dielectric constant, feature vector, support vector machine.

## I. INTRODUCTION

A large amount of coal gangue is produced during coal mining. Coal gangue is a kind of solid waste with a low carbon content, and accounts for 10%-15% of raw coal. The main components of coal are hydrocarbon active organic molecules, while the main components of coal gangue are $Al_2O_3$ and $SiO_2$. Coal gangue mixed with coal will not only reduce the quality of coal combustion, but also increase the emission of waste gas. To improve the quality of coal combustion and reduce the emission of poisonous and harmful gases, the separation of coal gangue from raw coal is an important problem in coal mine engineering.

Coal gangue recognition is the key technology of coal gangue separation. Hou *et al.* [6]–[8] analyzed the difference data between coal and coal gangue in terms of the surface texture and grayscale characteristics, and combined them with a classification algorithm to study coal gangue recognition. Because the texture and grayscale characteristics of coal and coal gangue are greatly affected by light, the recognition accuracy is not high. Liu *et al.* [9]–[13] studied the morphological differences between coal and coal

The associate editor coordinating the review of this manuscript and approving it for publication was Shuihua Wang.

gangue on the basis of studying texture and gray features, and introduced multifractal to extract the geometric features of coal gangue, but the extraction process of multifractals geometric features is complex and has poor adaptability. Alfarzaeai *et al.* [14]–[20] studied the near infrared spectrum, thermal infrared spectrum and multispectral characteristics of coal and coal gangue, and obtained high recognition accuracy in a laboratory environment using a neural network algorithm. However, this technology is not mature, and it is difficult to apply in practice because of the influence of ambient temperature and light. Zhao *et al.* [21], [22] studied the radiation characteristics and attenuation characteristics of X-rays and $\gamma$ -rays in coal and coal gangue. Coal gangue can be identified in essence through the attenuation characteristics of X-rays and $\gamma$-rays; however, the radiation produced by rays will cause physical harm to workers, and the maintenance cost of equipment is also high. Wang *et al.* [23] proposed a method of measuring volume by 3D laser scanning technology, which was combined with dynamic weighing technology to identify coal gangue. Because the volume is an estimated value, the measurement error is relatively large. Yang *et al.* [24], [25] studied the vibration signals of coal and coal gangue particles colliding with metal plates, and extracted the eigenvalues of the signals in combination with a machine learning algorithm to identify coal gangue, but damage identification, can reduce the quality of coal. Finding a recognition feature with high reliability, easy extraction and few side effects has become a difficult task in the current recognition of coal and coal gangue. Nelson *et al.* [26]–[29] studied the dielectric properties of pulverized coal, and found that the dielectric constant of pulverized coal decreases regularly with increasing frequency, which provides a reference for studying the dielectric properties of coal and coal gangue. Muhammad *et al.* [30]–[33] conducted cutting-edge and pioneering studies in signal desiccating, signal decomposition and machine learning, with strong references. In this paper, the differences between the dielectric properties of coal and coal gangue are studied, and a recognition method of coal and coal gangue based on dielectric properties is proposed. This method can realize nondestructive testing of coal and coal gangue. X-ray and $\gamma$-ray identification equipment, has high radiation intensity; the internal features of coal and coal gangue that cannot be perceived by image recognition can be obtained.

In this study, coal and gangue were obtained from the Huainan mining area, and the SVM intelligent classification model was trained by combining the dielectric constant characteristics of coal and gangue with the SVM. The test results show that the capacitance method has high accuracy and strong timeliness in identifying coal and gangue, and has great research prospects.

## II. SYSTEM IDENTIFICATION PRINCIPLE

Coal and gangue have different chemical compositions, which leads to their different dielectric constants. In a time-varying electromagnetic field, the dielectric constants of coal and gangue tend to decrease with increasing frequency and voltage. Based on the difference in the dielectric constants of coal and gangue, a capacitance identification system of coal and gangue is designed. A schematic diagram of the identification system is shown in Figure 1. The capacitor is composed of upper and lower electrode plates and a movable medium in its middle region, which can be coal or coal gangue. The signal generator adds applies a high frequency signal to the circuit, and changing the medium into coal or gangue will cause the response signals at both ends of the resistance to change. A data recorder is used to collect the response signals, which are sent to a PC to preprocess, denoise the response signals, extract eigenvalues and construct feature vectors, and then, the feature vectors are input into the SVM intelligent classification model to identify and classify the medium.

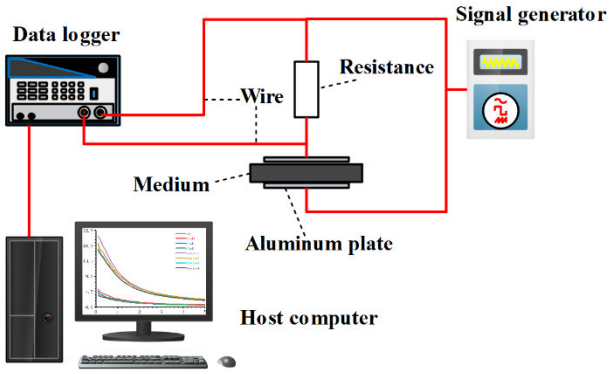


**FIGURE 1.** Schematic diagram of the identification system.

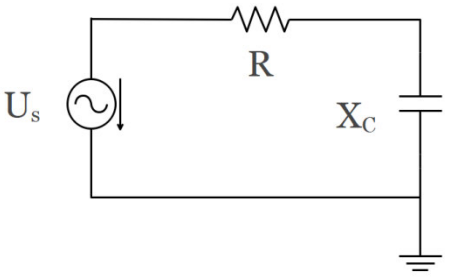


**FIGURE 2.** RC series circuit.

### A. ACQUISITION OF A RESPONSE SIGNAL

The schematic diagram of the identification system can be abstracted into a standard RC series circuit, as shown in Figure 2. In an RC series circuit, when the standard sinusoidal AC voltage $U_S$ is applied, the resistor R and capacitor $X_C$ will divide the voltage. The excitation voltage source was set as follows:

$$U_s = A\sqrt{2}\sin(2\pi ft + \varphi) \tag{1}$$

where $A$ is the amplitude of the AC voltage, $f$ is the frequency of the AC voltage, $t$ is time, and $\varphi$ is the initial phase angle, with $\varphi = 0$.

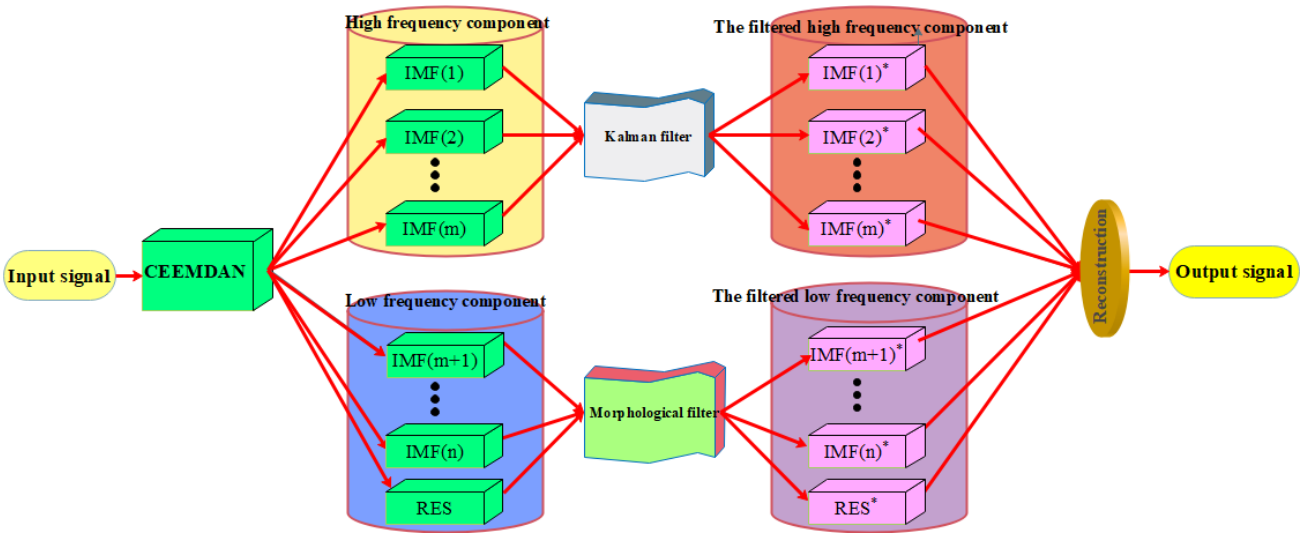


**FIGURE 3.** Improved CEEMDAN noise reduction flow chart.

In this RC series circuit, the effective value phasor of the input voltage $U_S$ is

$$\dot{U} = Ae^{j\varphi} \tag{2}$$

When $\varphi = 0$ at the standard sinusoidal AC voltage, $\dot{U} = \mathrm{A}$. In the circuit, the impedance of the resistor is R, and the impedance of the capacitor is

$$\mathrm{Z}_C = -jX_c \tag{3}$$

With $X_c = 1/(2\pi fC)$, we know that $\mathrm{Z}_C = -j\frac{1}{2\pi fC}$, and that effective value phasor of the voltage at both ends of resistor is

$$\dot{U}_R = \frac{R}{R - j\frac{1}{2\pi fC}}\dot{U} \tag{4}$$

By substituting the value of $\dot{U}$ into the formula and sorting it out, we obtain

$$\dot{U}_R = \frac{A2\pi fRC}{\sqrt{1 + (2\pi fRC)^2}} e^{j[\arctan(\frac{1}{2\pi fRC})]} \tag{5}$$

The effective voltage values at both ends of the resistor are as follows:

$$\mathrm{U}_R = \frac{A2\pi fRC}{\sqrt{1 + (2\pi fRC)^2}} \tag{6}$$

### B. RESPONSE SIGNAL PROCESSING

The response signals collected by the data recorder contain radio wave noise. To facilitate the later data analysis and feature extraction of the collected response signals, it is necessary to denoise the collected response signals [34]. CEEMDAN noise reduction has a good effect on nonlinear and nonstationary signals. The traditional CEEMDAN noise reduction method processes the IMF component dominated by high-frequency noise with a wavelet-like threshold, processes the IMF component dominated by useful signals with mathematical morphology filtering, and finally reconstructs the IMF and residual components after each processing step. Because of wavelet threshold processing, it is necessary to select the wavelet and set the threshold in advance, which is not adaptive and will lead to signal distortion [35]. In this paper, the Kalman filtering algorithm is introduced to improve the CEEMDAN denoising method. The IMF component dominated by high frequency noise is processed by Kalman filtering, and the IMF component dominated by useful signals is processed by mathematical morphology filtering. Finally, the IMF and residual components after each processing step are reconstructed. The improved CEEMDAN noise reduction process is shown in Figure 3.

### C. FEATURE EXTRACTION

The denoised sample data are imported into the feature extraction program of MATLAB. When the input excitation voltage and frequency are fixed, formula (13) shows that the dielectric constant is only related to the change in $\mathrm{U_R}$, but to calculate the value of the dielectric constant, multiple constant parameters need to be input. In future experiments, the structure of capacitors may vary with the size of coal and gangue samples. To simplify the process of feature extraction, only $\mathrm{U_R}$ and excitation frequency F representing the dielectric constant of each sample are extracted to form the feature vectors:

$$\boldsymbol{x} = [\mathbf{U}_{\boldsymbol{R}}, \boldsymbol{f}] \tag{7}$$

### D. SVM INTELLIGENT CLASSIFICATION MODEL

When it is necessary to identify and classify many samples in real time, an intelligent classification model needs to be established. The SVM takes a classification hyperplane as the decision surface to maximize the isolated edge between two classification objects. The SVM intelligent classification model to be established in this paper belongs to the SVM

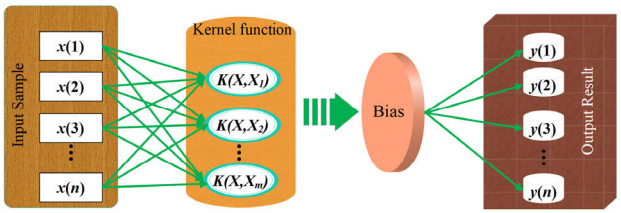


**FIGURE 4.** SVM model structure diagram.

linear dichotomy, and the structure of the model is shown in Figure 4.

SVM has good learning generalization ability in the pattern recognition of small sample data processing, and the algorithm itself is targeted at the dichotomy problem [36]. The specific form of the model is as follows:

Construct a training set of samples:

$$\mathrm{T} = \{(x_1, y_1), \cdots, (x_l, y_l)\} \in (X \times Y)^l \tag{8}$$

where $x_i \in X = R^n$, $y_i \in \{1, -1\}$ $(i = 1, 2, \cdots, l)$, and $x_i$ is the feature vector.

Select the linear kernel function $K\left(x, x'\right)$ and suitable parameter $C$, and construct and solve the optimization problem:

$$\begin{cases} \min\limits_{\alpha} \dfrac{1}{2} \sum\limits_{i=1}^{j} \sum\limits_{j=1}^{l} y_i y_j \alpha_i \alpha_j K\left(x_i, x_j\right) - \sum\limits_{j-1}^{l} \alpha_j \\ \sum\limits_{i=1}^{l} y_i \alpha_i = 0 \\ 0 \le \alpha_i \le C \end{cases} \tag{9}$$

Obtain the optimal solution:

$$\alpha^* = (\alpha_1^*, \cdots, \alpha_l^*)^T \tag{10}$$

Select a positive component of $\alpha^*$, $0 < \alpha_j^* < C$, and then calculate the threshold:

$$b^* = y_i - \sum\nolimits_{i=1}^{l} y_i \alpha_i^* K\left(x_i - x_j\right) \tag{11}$$

Build a decision function:

$$f\left(x\right) = sgn\left(\sum\nolimits_{i=1}^{l} \alpha_i^* y_i K\left(x, x_i\right) + b^*\right) \tag{12}$$

## III. STRUCTURAL DESIGN AND SIMULATION ANALYSIS OF THE POLAR PLATE

The dielectric constant of the material can be reflected in the capacitance calculation, and the noncontact measurement of the material can be made by using the capacitance method. According to physics, if the edge effect of a capacitor composed of two flat metal plates is not considered, the electric field distribution of the capacitor is shown in Figure 5-a, and the ideal calculation formula of its capacitance is

$$C_0 = \frac{\varepsilon_r S}{4\pi k d} \tag{13}$$

where $\varepsilon_r$ is the relative dielectric constant of the medium between two plates, $S$ is the relative effective area of two polar plates, $k$ is the electrostatic force constant, and $d$ is the distance between two polar plates.

In practical applications, the phenomenon of a divergent electric field at the edge of a capacitor is called the edge effect of the capacitor, and the thickness of the plate is an important factor affecting the edge effect of the capacitor [37]. Figure 5-b shows the electric field distribution when the edge effect of the plate is considered.

Formula (13) of the parallel plate capacitor is obtained by simplifying the derivation formula of the infinite round plate capacitor, and the real capacitance value also includes the stray capacitance caused by the edge effect.

$$\begin{aligned} \mathrm{C} &= \mathrm{C}_0 + \mathrm{C}_* \\ &= \varepsilon_0 \varepsilon_r \left\{ \frac{\pi r^2}{d} + \left[ \ln \frac{16\pi}{d} + 1 + f\left(\frac{h}{d}\right) \right] \right\} \\ &= \frac{\varepsilon_0 \varepsilon_r \pi r^2}{d} + \varepsilon_0 \varepsilon_r \left[ \ln \frac{16\pi}{d} + f\left(\frac{h}{d}\right) \right] \end{aligned} \tag{14}$$

where $h$ is the thickness of the polar plate, and $\varepsilon_0$ is the relative dielectric constant of a vacuum. The neglected stray capacitance value generated by the edge effect of capacitance is

$$\mathrm{C}_* = \varepsilon_0 \varepsilon_r \left[ \ln \frac{16\pi}{d} + f\left(\frac{h}{d}\right) \right] \tag{15}$$

Deviation $(\xi)$ caused by ignoring the edge effect of capacitance is

$$\xi = \frac{\mathrm{C}_*}{C} = \frac{\ln \frac{16\pi}{d} + f\left(\frac{h}{d}\right)}{\frac{\pi r^2}{d} + \ln \frac{16\pi}{d} + f\left(\frac{h}{d}\right)} \tag{16}$$

To study the influence of the edge effect of the electrode plate on the capacitor, three-dimensional modeling of the electrode plate and the medium to be measured is carried out in Maxwell software, and the electromagnetic simulation analysis of the model is carried out, as shown in Figure 6.

In the case when the plate distance of the capacitor is determined, the deviation $\xi$ is only affected by the thickness $h$ of the plates. The influence of plate thickness, $h$, on capacitance can be simulated and analyzed by Maxwell software. The thickness of the medium sample is 30 mm, and the diameter is approximately 120 mm. In the simulation experiment, the distance between plates is set to 30 mm; the plates are 10 mm long and 30 mm wide; The excitation voltage is set to 10 V; The plates are made of aluminum, the intermediate filling medium is customized coal, and the dielectric constant is 2.6; parametric scanning of the thickness $h$ of the plates is carried out from 0.5 mm to 10 mm. The curve of error $\xi$ changes with increasing f plate thickness, as shown in Figure 7. The error $\xi$ increases with the increasing plate thickness. When designing capacitors, the thickness of plates should be as small as possible if conditions permit, to reduce the influence of the edge effect on capacitance. The actual value of the corrected capacitor is

$$\mathrm{C} = \frac{\mathrm{C}_0}{(1 - \xi)} = \frac{\varepsilon_r S}{4\pi k d\,(1 - \xi)} \tag{17}$$

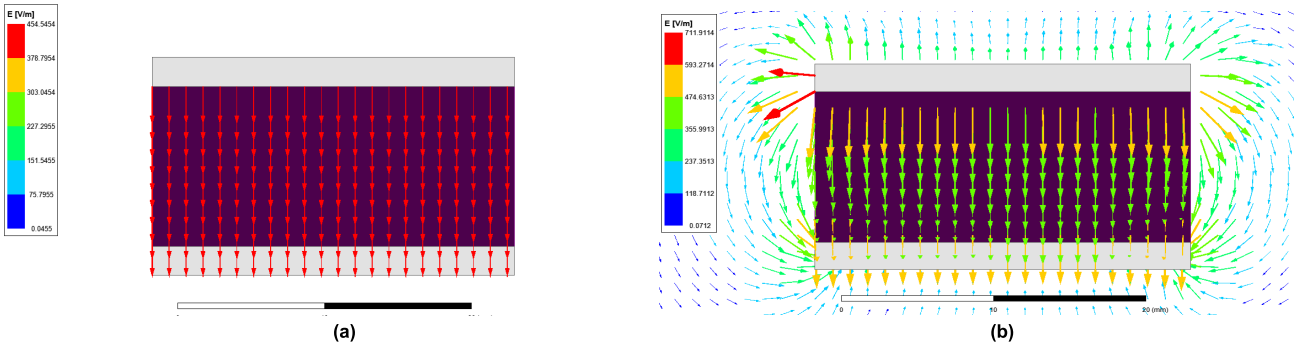


**FIGURE 5.** Comparative diagram of the capacitance electric field distribution in two cases: (a) the electric field distribution diagram without considering the edge effect of the plate; and (b) the electric field distribution diagram considering the edge effect of the plate.

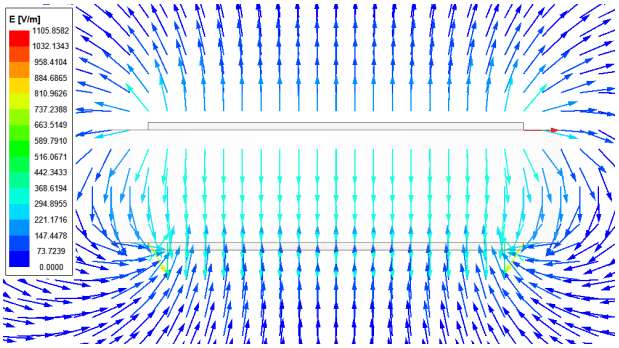


**FIGURE 6.** Simulation diagram of the capacitor model.

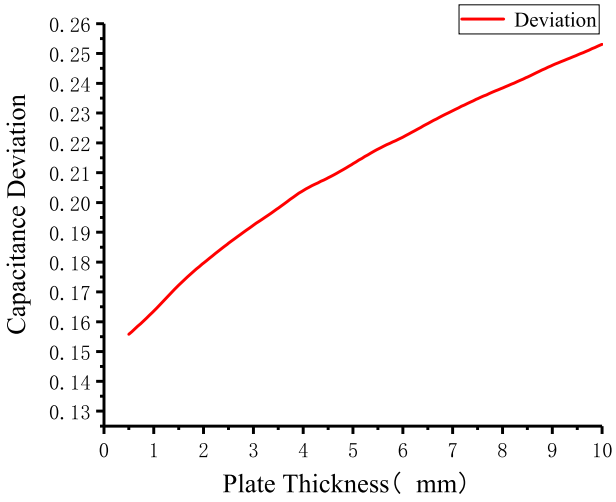


**FIGURE 7.** The curve of error with the thickness of plate.

By combining formula (6) and formula (17), the relative dielectric constant of the medium in the capacitor, the effective values of the voltage $U_R$ at both ends of the resistor R and the relationship between the frequency of the response signal can be obtained:

$$\varepsilon_r = \frac{2kd(1-\xi)\,U_R}{\sqrt{A^{2-}U_R^2}fRS} \tag{18}$$

Formula (18) shows that in the alternating RC series circuit, the effective values of the voltage at both ends of the resistor are measured. According to the structure parameters and excitation source parameters of the capacitor, the relative dielectric constant of the dielectric capacitor at a given frequency or voltage is calculated.

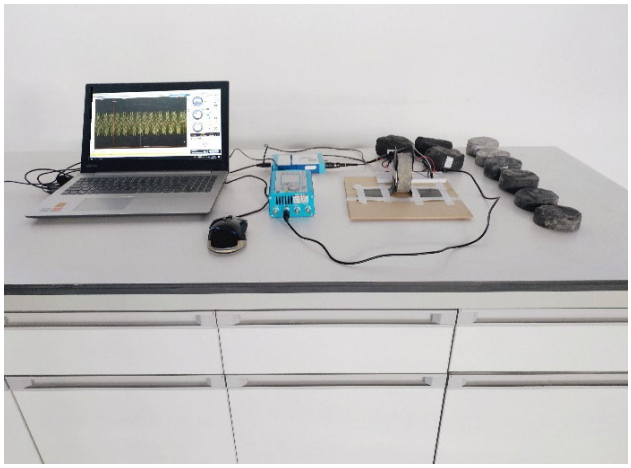

**FIGURE 8.** Recognition system.

## IV. DESIGN OF EXPERIMENT

### A. PREPARATION OF EXPERIMENTAL MATERIALS

The coal and gangue samples used in this experiment were collected from Zhujidong Coal Mine, Panji District, Huainan City, Anhui Province. To facilitate the experiment, 15 coal and gangue samples were cut and polished to form a round pie-shaped specimen with a diameter of 11 cm and a thickness of 3 cm. As shown in Figure 8, the identification system includes a signal generator, a computer, a data recorder, a constant value resistor, a plate capacitor, a circuit board and a number of Dupont lines. The parameters of the relevant components are shown in Table 1.

### B. THE INFLUENCE OF EXTERNAL CONDITIONS ON DIELECTRIC AND DIELECTRIC CONSTANTS

The dielectric constants of coal and gangue are affected by voltage and frequency in the AC circuit, and when the ambient temperature changes, the dielectric constant is also affected by temperature. Considering that a slow change in

**TABLE 1. Parameters corresponding to the components.**

| Components | Parameters |
|---|---|
| Signal generator | Model: FY2300-12M; Frequency resolution: 1μHz; Amplitude resolution: 1 mV. |
| Computer | Processor: Intel core i7-7500U CPU @ 2.70 GHz 2.90 GHz ; RAM: 4.00G. |
| Data recorder | Model: LOTO OSC482; Maximum sampling rate: 50 M;Bandwidth: 20 MHz. |
| Fixed value resistance | Brand: Risym; Types: Metal film resistor; Resistance: 1200 Ω. |
| Plate | Material: Aluminum; Size: 100 mm×30 mm×1 mm. |
| Circuit board | MB-102 Premium breadboard. |

temperature is not a suitable inducing factor, the influence of temperature on the dielectric constant is no longer considered, a contrast experiment is carried out at normal temperature, and only experiments studying the effect of voltage and frequency on the dielectric constant are carried out.

### 1) EXPLORE THE INFLUENCE OF EXCITATION SOURCE FREQUENCY ON DIELECTRIC CONSTANT

To reduce the requirement of capacitor insulation under AC power excitation, the output frequency of the signal generator is selected to be greater than 50kHz. The output voltage amplitude of the signal generator is set to 10.00 V; the duty ratio is 50.0%; and the initial phase is 0.00. Each group of experiments takes 100 kHz as the starting frequency and increases it by 100 kHz every time. The frequency of each frequency point and the effective value $U_R$ at both ends of resistor R at this frequency are recorded. When the input frequency reaches 5 MHz, the single-group experiment ends. Three kinds of media, air, coal and coal gangue, are measured, including one group of air media, three groups of coal media and four groups of coal gangue media. Fifty sampling points are collected for each group of specimens.

The curve showing the change in the effective value of the voltage $U_R$ at both ends of the resistor is shown in Figure 9 when the medium for each group of experiments is excited at different frequencies. Given that the thickness of the polar plate is 1 mm, we can obtain $\xi = 0.163$ from the curve of the error versus the thickness of the polar plate in the model simulation. By substituting the $U_R$ data and the known parameter values into formula (18), the curve of the dielectric constant $\varepsilon_r$ versus frequency is obtained, as shown in Figure 10. The characteristics of the curve conform to the law that the dielectric constant of matter decreases with the change in frequency. The observations indicate that the permittivities of coal and air are close to each other, and the change trends are similar. The permittivities of coal and gangue are obviously different and change.

To determine the excitation frequency when the difference between the permittivities of coal and coal gangue is the largest, the dielectric constants of the measured samples from the same category at the same frequency are averaged.

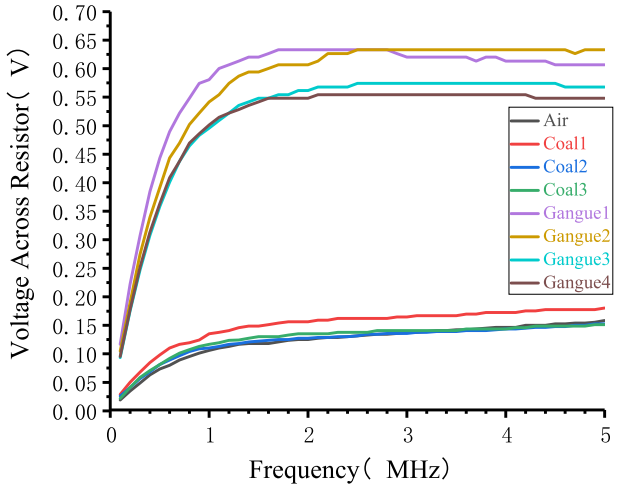


**FIGURE 9. The curve of $U_R$ versus frequency.**

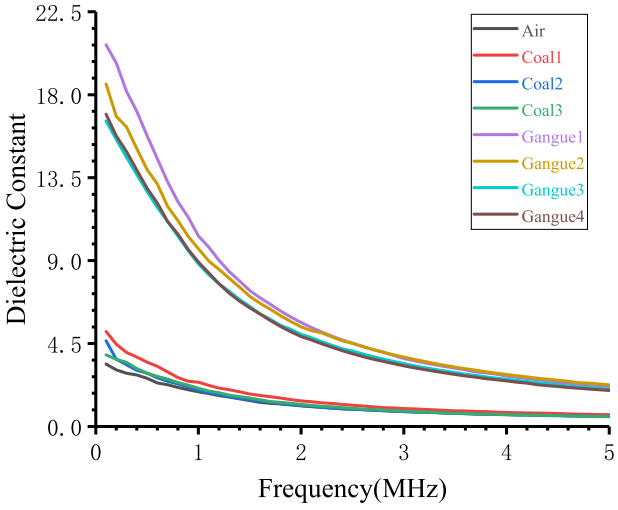


**FIGURE 10. The curve of the permittivity $\varepsilon_r$ versus frequency.**

The curve of the differences in the $\varepsilon_*$ values, the average dielectric constants of coal and coal gangue, versus frequency is shown in Figure 11. The $\varepsilon_*$ value of coal and coal gangue is the largest at a frequency of 100 kHz, and the identification characteristics of coal and coal gangue are the most obvious at this frequency.

### 2) EXPLORING THE INFLUENCE OF THE EXCITATION SOURCE VOLTAGE ON THE DIELECTRIC CONSTANT

The output voltage frequency of the signal generator is set as 100 kHz, the duty ratio is 50.0%, and the initial phase is 0.00°. Each group of experiments takes 1 V as the starting voltage, which increases by 0.5V each time. The value of each input voltage and the $U_R$ at both ends of resistor R under this voltage are recorded. When the input voltage reaches 20 V, the single-group experiment ends. Eight groups of samples of the abovementioned three kinds of media, air, coal and coal gangue, are measured, and 40 sampling points are collected from each group of samples. The curves showing the change in the dielectric constants of air, coal and coal

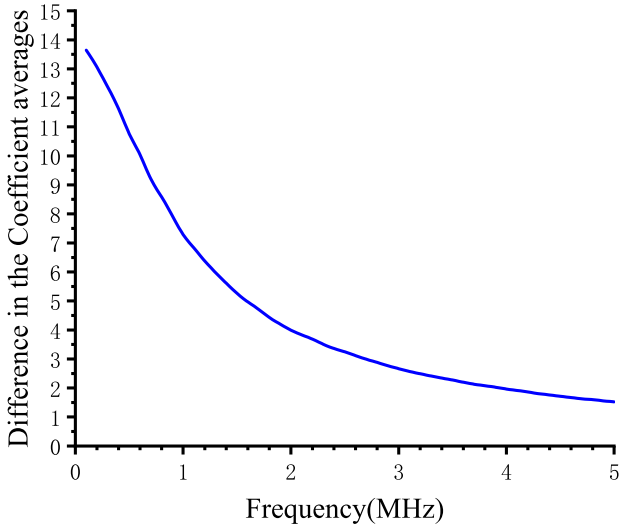


**FIGURE 11.** The curve of the difference in the average permittivity versus frequency.

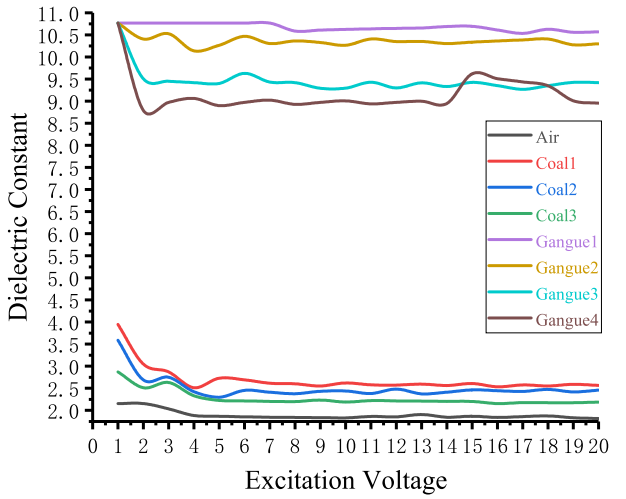


**FIGURE 12.** The curve of dielectric constant versus the excitation voltage.

gangue with voltage are shown in Figure 12. The dielectric constant tends to decrease with increasing voltage, but when the voltage is greater than 5 V, the dielectric constant is almost no longer affected by voltage. Therefore, when the voltage of the excitation source is greater than 5 V, the influence of voltage on the dielectric constant can be ignored.

## V. EXPERIMENTAL VERIFICATION AND DATA ANALYSIS

From the experiments studying the influence of voltage and frequency on air, coal and coal gangue, it can be seen that the dielectric constant characteristics of coal and air are similar and obviously different from those of coal gangue. Therefore, we only need to identify coal gangue to separate coal and gangue, so only coal and gangue are considered in the following experiments. According to the characteristic curves of the influence of frequency and voltage on the dielectric constant obtained from the above experiments, the excitation frequency of the excitation source is 100 kHz and the voltage

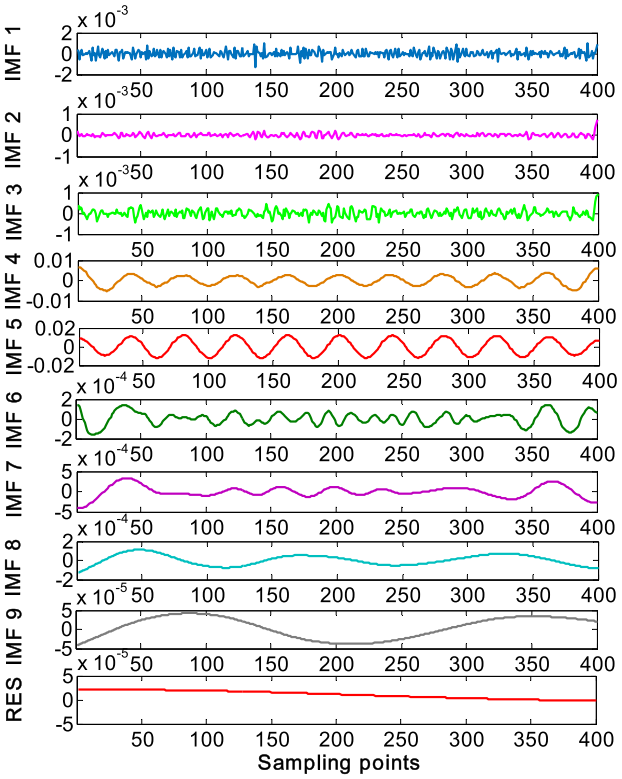


**FIGURE 13.** Modal component of a sample signal decomposed by CEEMDAN.

is 10 V, and the identification system is used to sample 15 coal samples and 15 coal gangue samples. Ten samples are taken for each specimen, the specimen is sampled once every 36° around the rotation axis, 400 sample points are collected every time, and the sample data are saved as CSV files.

Sample data are extracted from MATLAB software and decomposed by CEEMDAN. The CEEMDAN decomposition result of a single sample signal is shown in Figure 13, and IMF components are arranged in sequence according to their frequency. According to the IMF components, IMF1, IMF2 and IMF3 are high frequency components whose frequencies are higher than those of the excitation source, and the main radio wave noise is contained in the high frequency components. The measurement amplitude and frequency will be affected by high frequency noise, and then the recognition accuracy will be affected. A Kalman filter was used to filter IMF1, IMF2 and IMF3 components dominated by high-frequency noise, and a mathematical morphological filter was used to filter IMF components dominated by useful signals.

Finally, the IMF and residual components after each processing step are reconstructed. As shown in Figure 14, the improved CEEMDAN noise reduction effect is compared with the traditional CEEMDAN noise reduction effect.

Compared with that obtained by the traditional CEEMDAN denoising method, the signal obtained by the improved CEEMDAN denoising method has a higher signal-to-noise ratio (SNR) and lower root mean square error (RMSE). See Table 2 for specific parameter values.

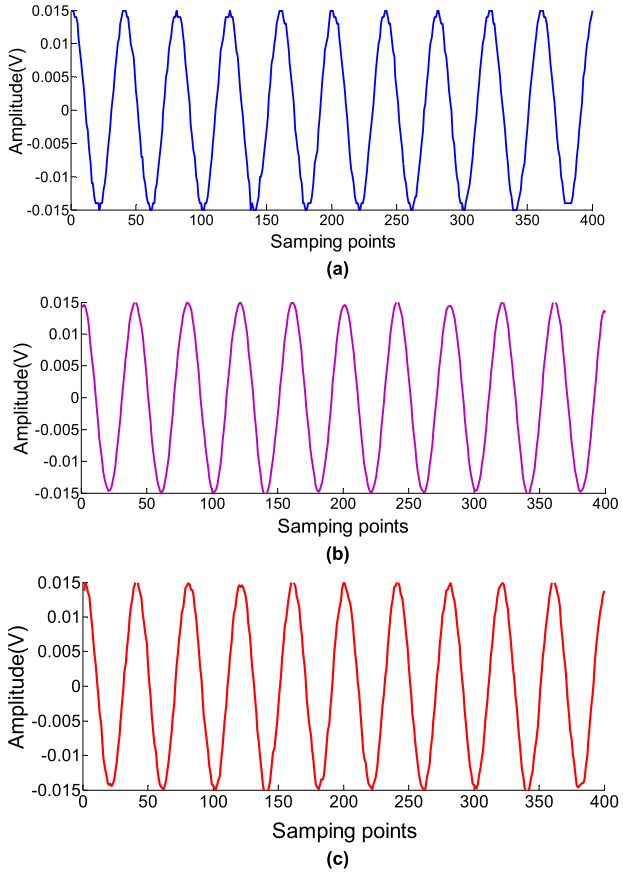


**FIGURE 14.** Modal component of a sample signal decomposed by CEEMDAN: (a) original signal; (b) CEEMDAN- wavelet threshold denoising;and (c) CEEMDAN- Kalman filter.

**TABLE 2.** The denoising effect values.

| Denoising methods | SNR | RMSE |
|---|---|---|
| CEEMDAN- wavelet threshold denoising | 13.9276 | 0.0013407 |
| CEEMDAN- Kalman filter | 14.0782 | 0.0010876 |

**TABLE 3.** Partial training samples.

| Training sample | label | $U_R$ | $f$ |
|---|---|---|---|
| Coal gangue | 1 | 0.015701 | 100 |
| Coal | 2 | 0.0019967 | 100 |
| Coal | 2 | 0.002264 | 100 |
| Coal gangue | 1 | 0.012648 | 100 |
| Coal | 2 | 0.0023108 | 100 |
| Coal gangue | 1 | 0.011095 | 100 |

With the improved CEEMDAN denoising method adopted, the complete useful signal can be obtained, and the noise component in the signal can be removed more effectively, which is helpful to improve the accuracy of the subsequent analysis of the response signal.

Two classification modes of coal and gangue are defined, and denoted as 2 and 1, respectively. Among the 300 samples collected, the 1st-150th samples belong to the first category,

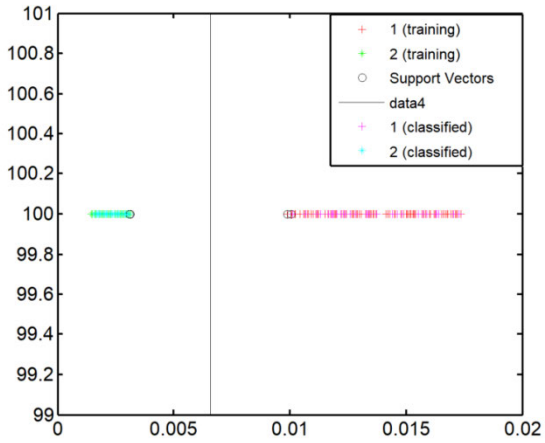


**FIGURE 15.** SVM intelligent classification model recognition results.

**TABLE 4.** Comparison of recognition effects.

| Intelligent classification model | Recognition accuracy | Recognition time/s |
|---|---|---|
| SVM intelligent classification model | 100% | 0.007916 |
| PNN neural network classification model | 100% | 0.043384 |
| LVQ neural network classification model | 100% | 0.214039 |

and the 151st-300th samples belong to the second category. A total of 120 samples from each category are selected to form the training set, and the remaining 30 samples from each category are selected to form the test set. Some samples of the test set are shown in Table 3, and the samples of coal and coal gangue are randomly arranged. The training set is input into the SVM training function for training, and the SVM intelligent classification model is constructed. The test set is input into the created SVM intelligent classification model, with 60 test samples of coal and gangue, and the classification results are shown in Figure 15. The classification accuracy of the SVM intelligent classification model is as high as 100%. To prove the efficiency of the SVM intelligent classification model, a comparative experiment between the PNN neural network intelligent classification model and LVQ neural network classification model is also carried out. The recognition and classification effects of the three classification models are shown in Table 4, and the recognition and classification accuracy of the PNN neural network intelligent classification model and LVQ neural network classification model can also reach 100%. This fully shows that it is feasible to identify coal gangue by the difference in the dielectric constant between coal and coal gangue. In terms of the processing time of test sets, the SVM intelligent classification model takes the shortest time, only 0.007916 s, with a higher real-time performance.

## VI. CONCLUSION

According to the differences in the dielectric properties coal and gangue, the dielectric constants of coal and gangue are first proposed as the identification characteristics, which

provides a new method to identify coal and gangue. In this paper, a capacitance identification method based on coal and gangue with regular shapes is conceived, and remarkable recognition and classification results are obtained by combining the SVM intelligent classification model. The main contributions of this paper are as follows:

1) The capacitance identification model of coal and gangue is established, and the finite element simulation analysis of the capacitor model is carried out. The influence of the edge effect caused by plate thickness on the calculation of the capacitance value is obtained, and the calculation formula of the capacitance value is modified to accurately calculate the capacitance value of the capacitor when the medium changes.

2) The capacitance identification system of coal and gangue is designed. The circuit of the identification system is analyzed by the phasor method, and the relationship between the dielectric constant and the structural parameters of the model and the electrical parameters of the identification system is obtained by combining the modified calculation formula of the capacitance. The change in the dielectric constants of coal and gangue with changing in the frequency and voltage of the excitation source is explored by using this identification system, which is used to guide select the frequencies and voltages that cause obvious differences between coal and gangue.

3) Combined with the Kalman filter, the traditional CEEMDAN denoising method is improved, the sample signal is used for verification, and a processing signal with a high signal-to-noise ratio and low root mean square error is obtained.

4) The recognition and classification effects reach 100%. The recognition accuracy of the SVM intelligent classification model for 60 test samples is as high as 100%, and the processing time is only 0.007916 s. The feasibility of identifying coal gangue by the capacitance method is ensured in terms of accuracy and real-time, which provides a theoretical reference for research on identifying coal and coal gangue with irregular shapes by the capacitance method.

## REFERENCES


[1] F. Pan, X. Lu, T. Wang, Y. Wang, Z. Zhang, and Y. Yan, "Triton X-100 directed synthesis of mesoporous $\gamma-Al_2O_3$ from coal-series kaolin," *Appl. Clay Sci.*, vol. 85, pp. 31–38, Nov. 2013.

[2] J. Zuber, N. Dittrich, P. Rathsack, and C. Vogt, "Direct mass spectrometric analysis of solid coal samples using laser desorption/ionization Fourier transform ion cyclotron resonance mass spectrometry," *Energy Fuels*, vol. 34, no. 8, pp. 9573–9584, Aug. 2020.

[3] L. Han, W. Ren, B. Wang, X. He, L. Ma, Q. Huo, J. Wang, W. Bao, and L. Chang, "Extraction of $SiO_2$ and $Al_2O_3$ from coal gangue activated by supercritical water," *Fuel*, vol. 253, pp. 1184–1192, Oct. 2019.

[4] J. Xiao, F. Li, Q. Zhong, H. Bao, B. Wang, J. Huang, and Y. Zhang, "Separation of aluminum and silica from coal gangue by elevated temperature acid leaching for the preparation of alumina and SiC," *Hydrometallurgy*, vol. 155, pp. 118–124, May 2015.

[5] R. Gao, Z. Sun, W. Li, L. Pei, Y. Hu, and L. Xiao, "Automatic coal and gangue segmentation using U-Net based fully convolutional networks," *Energies*, vol. 13, no. 4, p. 829, Feb. 2020.

[6] W. Hou, "Identification of coal and gangue by feed-forward neural network based on data analysis," *Int. J. Coal Preparation Utilization*, vol. 39, no. 1, pp. 33–43, Jan. 2019.

[7] D. Dou, D. Zhou, J. Yang, and Y. Zhang, "Coal and gangue recognition under four operating conditions by using image analysis and relief-SVM," *Int. J. Coal Preparation Utilization*, vol. 40, no. 7, pp. 473–482, Jul. 2020.

[8] M. Li, Y. Duan, X. He, and M. Yang, "Image positioning and identification method and system for coal and gangue sorting robot," *Int. J. Coal Preparation Utilization*, vol. 40, pp. 1–19, May 2020, doi: 10.1080/19392699.2020.1760855.

[9] K. Liu, X. Zhang, and Y. Chen, "Extraction of coal and gangue geometric features with multifractal detrending fluctuation analysis," *Appl. Sci.*, vol. 8, no. 3, p. 463, Mar. 2018.

[10] C. Fu, F. Lu, and G. Zhang, "Discrimination analysis of coal and gangue using multifractal properties of optical texture," *Int. J. Coal Preparation Utilization*, vol. 40, pp. 1–13, Jul. 2020, doi: 10.1080/19392699.2020.1789974.

[11] Z. Sun, W. Lu, P. Xuan, H. Li, S. Zhang, S. Niu, and R. Jia, "Separation of gangue from coal based on supplementary texture by morphology," *Int. J. Coal Preparation Utilization*, vol. 39, pp. 1–17, Mar. 2019, doi: 10.1080/19392699.2019.1590346.

[12] H. Zou and R. Jia, "Visual positioning and recognition of Gangues based on scratch feature detection," *Traitement du Signal*, vol. 36, no. 2, pp. 147–153, Jul. 2019.

[13] Y. Pu, D. B. Apel, A. Szmigiel, and J. Chen, "Image recognition of coal and coal gangue using a convolutional neural network and transfer learning," *Energies*, vol. 12, no. 9, p. 1735, May 2019.

[14] M. S. Alfarzaeai, Q. Niu, J. Zhao, R. M. A. Eshaq, and E. Hu, "Coal/gangue recognition using convolutional neural networks and thermal images," *IEEE Access*, vol. 8, pp. 76780–76789, 2020.

[15] L. Zou, X. Yu, M. Li, M. Lei, and H. Yu, "Nondestructive identification of coal and gangue via near-infrared spectroscopy based on improved broad learning," *IEEE Trans. Instrum. Meas.*, vol. 69, no. 10, pp. 8043–8052, Oct. 2020.

[16] L. Song, S. Liu, M. Yu, Y. Mao, and L. Wu, "Research on coal and gangue classification method based on combined analysis of visible-near infrared and thermal infrared spectroscopy," *Spectrosc. Spectral Anal.*, vol. 37, no. 2, pp. 416–422, Feb. 2017.

[17] R. M. A. Eshaq, E. Hu, M. Li, and M. S. Alfarzaeai, "Separation between coal and gangue based on infrared radiation and visual extraction of the YCbCr color space," *IEEE Access*, vol. 8, pp. 55204–55220, 2020.

[18] D. P. Tripathy and K. G. R. Reddy, "Novel methods for separation of gangue from limestone and coal using multispectral and joint color-texture features," *J. Inst. Eng. (India), Ser. D*, vol. 98, no. 1, pp. 109–117, Apr. 2017.

[19] F. Hu, M. Zhou, P. Yan, K. Bian, and R. Dai, "Multispectral imaging: A new solution for identification of coal and gangue," *IEEE Access*, vol. 7, pp. 169697–169704, 2019.

[20] W. Lai, M. Zhou, F. Hu, K. Bian, and H. Song, "A study of multispectral technology and two-dimension autoencoder for coal and gangue recognition," *IEEE Access*, vol. 8, pp. 61834–61843, 2020.

[21] Y. D. Zhao and X. He, "Recognition of coal and gangue based on X-ray," *Appl. Mech. Mater.*, vols. 275–277, pp. 2350–2353, Jan. 2013.

[22] N. Zhang and C. Liu, "Radiation characteristics of natural gamma-ray from coal and gangue for recognition in top coal caving," *Sci. Rep.*, vol. 8, no. 1, pp. 1–9, Jan. 2018.

[23] W. Wang and C. Zhang, "Separating coal and gangue using three-dimensional laser scanning," *Int. J. Mineral Process.*, vol. 169, pp. 79–84, Dec. 2017.

[24] Y. Yang, Q. Zeng, and G. Yin, "Vibration test of single coal gangue particle directly impacting the metal plate and the study of coal gangue recognition based on vibration signal and stacking integration," *IEEE Access*, vol. 7, pp. 106783–106804, Aug. 2019.

[25] Y. Yang, Q. Zeng, L. Wan, and G. Yin, "Influence of coal gangue volume mixing ratio on the system contact response when multiple coal gangue particles impacting the metal plate and the study of coal gangue mixing ratio recognition based on the metal plate contact response and the multi-information fusion," *IEEE Access*, vol. 8, pp. 102373–102398, 2020.

[26] S. O. Nelson, S. R. Beck-Montgomery, and G. E. Fanslow, "Camouflage Covert Communication in Air by Imitating Cricket's Sound," *J. Microw. Power.*, vol. 16, n.3-4, pp. 319–326, Dec. 1981.

[27] J.-C. Giuntini, J.-V. Zanchetta, and S. Diaby, "Characterization of coals by the study of complex permittivity," *Fuel*, vol. 66, no. 2, pp. 179–184, Feb. 1987.

[28] I. Brach, J. Giuntini, and J. Zanchetta, "Real part of the permittivity of coals and their rank," *Fuel*, vol. 73, no. 5, pp. 738–741, May 1994.

[29] J. M. Forniés-Marquina, J. C. Martín, J. P. Martínez, J. L. Miranda, and C. Romero, "Dielectric characterization of coals," *Can. J. Phys.*, vol. 81, no. 3, pp. 599–610, Mar. 2003.

[30] M. T. Sadiq, X. Yu, Z. Yuan, and M. Z. Aziz, "Motor imagery BCI classification based on novel two-dimensional modelling in empirical wavelet transform," *Electron. Lett.*, vol. 56, no. 25, pp. 1367–1369, Dec. 2020, doi: 10.1049/el.2020.2509.
[31] Z. Fan, M. Jamil, M. T. Sadiq, X. Huang, and X. Yu, "Exploiting multiple optimizers with transfer learning techniques for the identification of COVID-19 patients," *J. Healthcare Eng.*, vol. 2020, pp. 1–13, Nov. 2020, doi: 10.1155/2020/8889412.
[32] M. T. Sadiq, X. Yu, Z. Yuan, Z. Fan, A. U. Rehman, G. Li, and G. Xiao, "Motor imagery EEG signals classification based on mode amplitude and frequency components using empirical wavelet transform," *IEEE Access*, vol. 7, pp. 127678–127692, 2019.
[33] M. T. Sadiq, X. Yu, and Z. Yuan, "Exploiting dimensionality reduction and neural network techniques for the development of expert brain-computer interfaces," *Expert Syst. Appl.*, vol. 164, no. 3, Feb. 2021, Art. no. 114031, doi: 10.1016/j.eswa.2020.114031.
[34] J. Jiang, J. Xu, F. Duan, X. Wang, W. Liu, and X. Fu, "Camouflage covert communication in air by imitating Cricket's sound," *IEEE Access*, vol. 8, pp. 71840–71850, 2020.
[35] L. Chen, J. Wang, Z. Sun, T. Huang, and F. Wu, "Smoothing photovoltaic power fluctuations for cascade hydro-PV-pumped storage generation system based on a fuzzy CEEMDAN," *IEEE Access*, vol. 7, pp. 172718–172727, 2019.
[36] J. Bao, J. Nie, C. Liu, B. Jiang, F. Zhu, and J. He, "Improved blind spectrum sensing by covariance matrix cholesky decomposition and RBF-SVM decision classification at low SNRs," *IEEE Access*, vol. 7, pp. 97117–97129, 2019.
[37] B. Wells, E. Baker, A. Farwell, H. Foster, X. Gao, B. Gruber, E. Jones, D. Vu, S. Xu, and J. Ye, "An adjustable parallel-plate capacitor instrument—Test of the theoretical capacitance formula," *Amer. J. Phys.*, vol. 84, no. 9, pp. 723–726, Sep. 2016.

**YONGCUN GUO** received the Ph.D. degree from the University of Science and Technology of China. He is currently a Professor with the Anhui University of Science and Technology. His research interests include mine robot, intelligent mining equipment, and photoelectric detection.

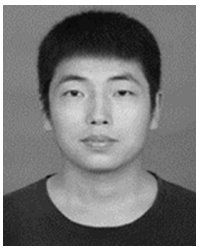

**XINQUAN WANG** is currently pursuing the Ph.D. degree with the Anhui University of Science and Technology. His research interests include pattern recognition, machine learning, and photoelectric recognition.

**SHUANG WANG** received the Ph.D. degree in mine electromechanical engineering from the Anhui University of Science and Technology, in 2018. She is currently a Lecturer with the Anhui University of Science and Technology. Her research interests include intelligent mining equipment, magnetic drive and magnetic levitation technology, and mine robot.

**KUN HU** received the Ph.D. degree in mine electromechanical engineering from the Anhui University of Science and Technology, in 2012. He is currently a Professor with the Anhui University of Science and Technology. His research interests include intelligent mining technology and equipment, magnetic levitation and magnetic transmission technology, and mining robot.

**WENSHAN WANG** is currently pursuing the Ph.D. degree with the Anhui University of Science and Technology. His research interests include permanent magnet variable frequency motor, smart steel technology, and intelligent mining equipment.